2024 IEEE International Conference on Robotics and Automation (ICRA 2024)
May 13-17, 2024. Yokohama, Japan

Empirical Study of Ground Proximity Effects for Small-scale Electroaerodynamic Thrusters

Grant Nations[1], C. Luke Nelson[2] and Daniel S. Drew[3]

***Abstract*— Electroaerodynamic (EAD) propulsion, where thrust is produced by collisions between electrostatically-accelerated ions and neutral air, is a potentially transformative method for indoor flight owing to its silent and solid-state nature. Like rotors, EAD thrusters exhibit changes in performance based on proximity to surfaces. Unlike rotors, they have no fragile and quickly spinning parts that have to avoid those surfaces; taking advantage of the efficiency benefits from proximity effects may be a route towards longer-duration indoor operation of ion-propelled fliers. This work presents the first empirical study of ground proximity effects for EAD propulsors, both individually and as quad-thruster arrays. It focuses on multi-stage ducted centimeter-scale actuators suitable for use on small robots envisioned for deployment in human-proximal and indoor environments. Three specific effects (ground, suckdown, and fountain lift), each occurring with a different magnitude at a different spacing from the ground plane, are investigated and shown to have strong dependencies on geometric parameters including thruster-to-thruster spacing, thruster protrusion from the fuselage, and inclusion of flanges or strakes. Peak thrust enhancement ranging from 300 to 600% is found for certain configurations operated in close proximity (0.2 mm) to the ground plane and as much as a 20% increase is measured even when operated centimeters away.**

I. Introduction

The small size of micro air vehicles (MAVs) makes them well-suited to applications requiring operation in constrained environments, including cluttered and / or indoor inspection and mapping [1]–[4], cave and subsurface complex exploration [5], [6], and warehousing [7]–[9]. These contexts demand high levels of maneuverability and trajectory precision to avoid damage to the vehicle or the environment—or to people, if operated near them. At the same time, scaling challenges (e.g., with propeller aerodynamics, motor efficiency, and battery power density) make the achievable flight duration for MAVs prohibitively short, precluding their more widespread adoption [10], [11]. Proximity to surfaces during flight affects the aerodynamic performance of all flying vehicles; there are a range of beneficial and deleterious effects depending on airfoil, actuator, and angle (e.g., if the surface is above, below, or to the side of the vehicle). Properly accounting for these effects is critical for designing robust and safe controllers, and they can have a potentially large impact on energy efficiency.

[1]Kahlert School of Computing, University of Utah, Salt Lake City, UT 84112, USA
[2]Department of Mechanical Engineering, University of Utah, Salt Lake City, UT 84112, USA
[3]Department of Electrical and Computer Engineering, University of Utah, Salt Lake City, UT 84112, USA
Corresponding author: Daniel S. Drew, daniel.drew@utah.edu

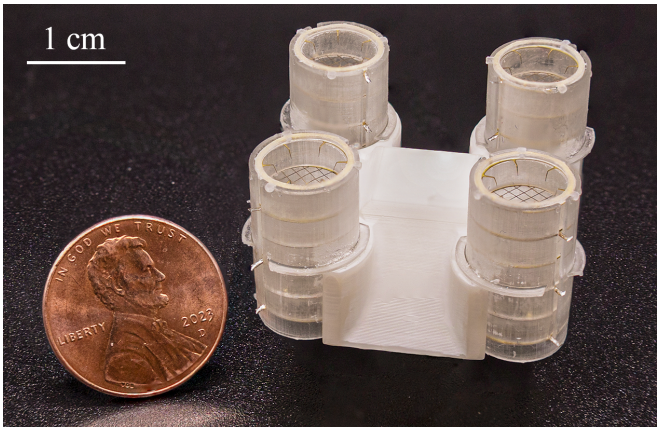

Fig. 1. Four ducted thrusters arranged in a "quadthruster" configuration, with 45° strakes extending down to form a skirt between them in order to minimize suckdown when in proximity to the ground. This design is shown to improve thrust by over 60% in close proximity to the ground, avoid any region of decreased thrust from suckdown, and still produce up to a 20% thrust benefit from fountain lift when further from the ground plane.

Electroaerodynamic (EAD) propulsion, where thrust is produced through the momentum-transferring collisions between charged particles accelerated in an electric field and neutral air molecules (Fig. 2), is an attractive mechanism for MAVs due to its silent and solid-state nature. Several small (i.e., centimeter-scale) robots have already been demonstrated which take advantage of EAD (also known as electrohydrodynamic, or EHD) actuators, capable of flying, rolling, hopping, or a combination thereof [12]–[15]. These robots are particularly well-suited for use in human-proximal environments in order to avoid the negative health and productivity outcomes caused by exposure to consistent loud noise, like that produced by rotorcraft [16]–[20]. Specific application spaces which would benefit from this unique feature of silent thrust production include urban package delivery, defense and intelligence operations, and wildlife tracking. Additionally, as they have no mechanical moving parts, EAD actuators are also safer to operate close to surfaces as compared to fragile rotors or flapping wings.

Despite a clear need, there has been no study of proximity effects as they apply to EAD propulsors to date. Here, we consider multi-staged ducted EAD thrusters suitable for small robots. The aerodynamic properties of EAD-based systems differ significantly from traditional ones; for example, they do not involve wing tip vortices on the actuator itself, the generation and stability of which are significantly impacted by surface proximity [21], [22]. The electrostatic force which accelerates the ions between collisions with

air is also largely decoupled from aerodynamics at realistic freestream velocities given the high velocities of ions (on the order of 100 m/s). To allow room for a detailed empirical investigation of ground proximity effects (i.e., the aerodynamic phenomena present when actuator exhaust is pointed at a nearby surface) for single- and quad-EAD thruster arrangements (e.g., Fig. 1), the reader is directed to prior work for further detail on EAD propulsion in general [12], [23], [24]. Expressions for thrust and thrust efficiency in N/W based on a simplified one dimensional theory for space charge limited discharges, where μ is the ion mobility, E is the average drift field magnitude, and v is the free-stream velocity, are given below [25], [26]. Although often used during modeling and characterization, they fail to capture aerodynamic and proximity effects.

$$F = \frac{Id}{\mu} = \frac{9}{8}\epsilon_0 A E^2 \quad (1) \qquad \eta = \frac{1}{\mu E + v} \quad (2)$$

The primary contribution of this work is a first-ever empirical investigation of ground proximity effects for EAD thrusters. It includes experiments looking at the impact of factors including distance from the ground, Reynolds number, inter-thruster spacing, thruster protrusion from the fuselage, and inclusion of strakes on measured thrust and thrust efficiency. Our results serve as an initial confirmation of which ground proximity effects are of primary importance for EAD-propelled robots and point towards fruitful future directions for experimentation and model development. We show that ground effects can be a net efficiency gain or loss depending on arrangement and surface distance, and show that it can increase static thrust by as much as 600% in specific configurations, or decrease it by as much as 20% in others. The magnitude of this effect means that it should not be ignored in future studies of EAD-propelled MAVs, and opens the door to entirely new designs for high-efficiency vehicles (e.g., ion-propelled micro-hovercraft).

II. Background and Related Work

This section attempts to succinctly describe the mechanisms by which ground proximity affects aerodynamic performance in general terms before pointing towards relevant related work in the domain of MAVs. Information on electrohydrodynamic and electroaerodynamic ground proximity effects more specifically is not included because it has not yet been investigated in the academic literature.

A. Physical Basis of Ground Proximity Effects

As with most aerodynamic phenomena, ground proximity effects can be explained at several levels of complexity, and their specifics are closely tied to the physical embodiment (e.g., actuator type and placement, fuselage shape) of the vehicle. The three primary effects of interest are the pressure ground effect (what is often referred to as "the" ground effect), suckdown, and fountain lift (Fig. 3).

In general, the *ground effect* refers to the apparent increase in thrust or lift experienced by an aircraft when in close proximity to the ground. It has been shown to affect fixed-wing, flapping-wing, rotory, and jet-powered vehicles across scales [21], [27]–[30]. While varying explanations exist, those focused on airfoil tip vortex reduction and increased leading-edge streamline curvature, for example, fail to account for the ground effect shown in jet engines without airfoils. The method of images, where a virtual source is mirrored across the ground plane to represent ground reaction forces, is mathematically satisfying and has been shown to accurately predict lift [31]. Simply, increased proximity to the plane results in a more vertical center-duct streamline and higher velocity induced wall jet, which is reflected in the mirror image to produce a larger ground reaction force in the direction of lift.

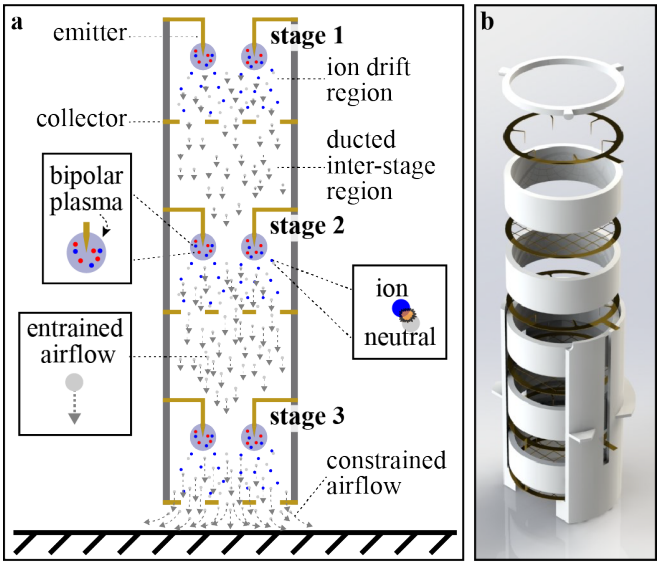

Fig. 2. **(a)** Schematic view of a three-stage electroaerodynamic ducted actuator. A high potential applied between the "emitter" and "collector" electrodes ignites a local plasma from which ions are ejected. These ions drift in the electric field towards the collector, and frequent momentum-transferring collisions with neutral air molecules along the way result in an entrained air jet. Successive stages increase the velocity of the air as it passes through the duct. **(b)** Render of the three-stage ducted devices used in this work, where UV-laser micromachined brass electrodes are integrated with SLA-printed ducts in an adhesiveless process. Design, fabrication, and assembly of these devices is drawn from prior work [24].

Proximity to a surface is not always beneficial; vertical and / or short takeoff-and-landing (V/STOL) aircraft also experience a negative effect known as *suckdown*. This comes as a result of the vehicle's actuators entraining and accelerating air vertically downward and around the bottom edges of the aircraft (red streamlines shown in Fig. 3b), creating an area of low pressure beneath the fuselage and a net "suction" pressure towards the plane [28]. Viscous mixing between the entrained air and the jet exhaust also reduces jet thrust when the change in velocity is propagated through the streamline [32].

Finally, in multi-rotor and multi-jet V/STOL aircraft, the wall jets produced by neighboring propulsors can collide and redirect beneath the aircraft to produce a vertical airflow which impacts the bottom of the fuselage and produces a

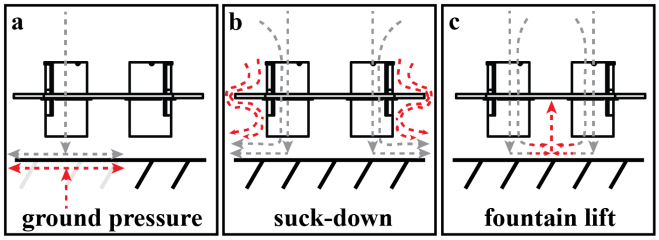

Fig. 3. Relevant proximity effects include **(a)** the ground effect, where high pressure buildup from the exhaust causes a net thrust-positive reaction force, **(b)** suckdown, where the radial wall jet entrains and accelerates air flowing over the fuselage, and **(c)** fountain lift, where adjacent wall jets collide and redirect to push against the underside of the fuselage. In these schematics, grey streamlines indicate relevant actuator outlet flow and red ones indicate induced flow or pressure.

net upward force known as *fountain lift*. The magnitude of this effect is a complicated function of jet decay rate, inter-actuator geometry, and the ratio between wall distance and jet diameter (at least) [33]. Fountain lift can also arise from reflections of individual thruster exhaust depending on collimation and angle-of-attack [34].

B. Ground Effects in Small Rotorcraft

The most salient related work includes other empirical studies looking at proximity effects for small (i.e., centimeter-scale) rotors and rotorcraft. While proximity effects are typically measured as functions of the dimensionless parameter distance-to-rotor radius, z/r, where z represents the distance between the ground plane and the thruster's outlet and r represents the actuator radius, there is a strong Reynolds number dependence for rotorcraft which makes analytical models used in practice for large vehicles (e.g., the Cheeseman model [35]) inaccurate for small ones. Besides the obvious difference of using EAD thrusters and not rotors, our work also notably investigates by far the smallest diameter propulsor of the studies we were able to find. In practice, this means that a low z/r ratio for our devices is a proportionally lower actual distance from the ground plane.

For example, Conyers et al. investigated the change in thrust in- and out- of ground effect for nine inch diameter rotors in isolation and in quadrotor arrangements [21], finding peak thrust enhancement of around 15% and 20%, respectively, below a z/r ratio of about unity. They also found evidence for fountain lift (with an approximately 5% benefit) for appropriately spaced quadthruster arrangements. Our work differs in that we show coarse control over fountain lift region location and magnitude via geometric parameters, and also investigate suckdown effects that are not apparent with their rotors. Dekker et al. investigated dual-rotor arrangements in close ground proximity, directly visualizing and confirming the presence of fountain flow [36]. A focus of their work was on predicting fountain flow re-ingestion by the propellers, which is not possible given the (relatively) long, ducted nature of our EAD thrusters. Jardin et al. used a single isolated microrotor propeller (radius 12.5 cm) to measure and model the ground effect, finding a peak thrust enhancement of approximately 75% in close proximity to the plane [37]. They also found a strong dependence on rotor pitch angle; although the analogous thruster angle of attack was not studied in this work, it is clear that it could be important. A review article by Matus-Vargas et al. [38] contains many more examples of modeling and empirical efforts for rotorcraft in the ground effect, though primarily for much larger vehicles.

Various authors have proposed quadrotor control architectures and / or physical embodiment which seek to take advantage of surface proximity to improve flight endurance [39]–[41]. We view this as an exciting future direction for EAD-propelled robots.

III. Methods

A. Thrusters

The individual EAD thrusters used in this study are nearly identical to those recently presented by Nelson and Drew [24], with modifications made only to the mounting structure. A single thruster consists of three ducted stages (as shown in Fig. 2) with an inner diameter of 8 mm and a total height of 17.6 mm. Succinctly, duct structures are fabricated via stereolithographic (SLA) printing, active electrodes are UV-laser micromachined, and the components are integrated using mechanical affordances and an adhesiveless locking system; further design, fabrication, and assembly details are omitted here for brevity but can be found in [24]. These thrusters have been found to have among the highest thrust densities recorded for any propulsor at this scale, with exhaust velocities approaching 5 m/s.

Inspired by prior work on centimeter-scale EAD-propelled robots [12], devices are assembled into "quadthruster" configurations using SLA-printed fuselage plates (Formlabs Form 3+, Rigid 10k resin) with printed locking clips (the latter are omitted from Fig. 4 for clarity). Controlled geometric parameters, which will be referenced throughout subsequent sections, are labeled in Fig. 4a (left) and include the thruster radius, r, the inter-thruster spacing, s, the thruster protrusion from the fuselage, h, and the distance from thruster exhaust to the ground plate, z.

B. Experimental Setup

The automated experimental testbed is constructed from a modified Ender 3 Pro 3D printer (Fig. 4, right). The extruder and X-axis stepper are replaced with a 230 mm by 230 mm by 6.35 mm Delrin acetal plastic plate, secured to the extruded aluminum frame with countersunk M5 bolts. This plate acts as the ground, and is lowered or raised to the desired z value using G-code commands sent from a Python script. The device under test is secured 53 mm above a FUTEK LSB200 S-Beam load cell in a rigid SLA-printed mount designed for unobstructed airflow, with thruster exhausts facing upwards towards the ground plate.

Voltage is applied to devices using a Spellman High Voltage SL8P programmable high-voltage power supply with a separate Python-controlled variable power supply connected to its remote inputs. Load cell readings are recorded in a separate thread at an interval of 100 mS. Voltages from the

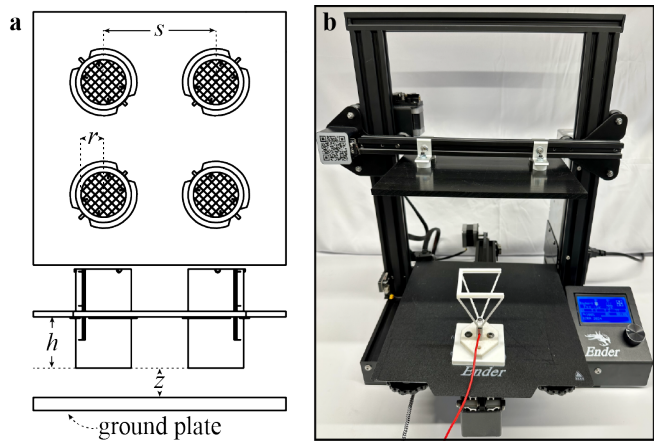

Fig. 4. **(a)** Schematic illustrating geometric parameters of interest, including the inter-thruster spacing s, thruster radius r, thruster protrusion from the fuselage h, and the distance from the thruster exhaust to the ground plate z. **(b)** The automated test setup constructed from a modified 3D printer synchronizes current-voltage and force-voltage data acquisition with precise movement of the ground plate. An entire experimental suite (i.e., every desired z/r value) can be initiated with a single command. The thruster is positioned with the exhaust facing up towards a ground plane. Note that, despite the orientation, this differs from the "ceiling" effect which depends on the *inlet* being next to the ground plane.

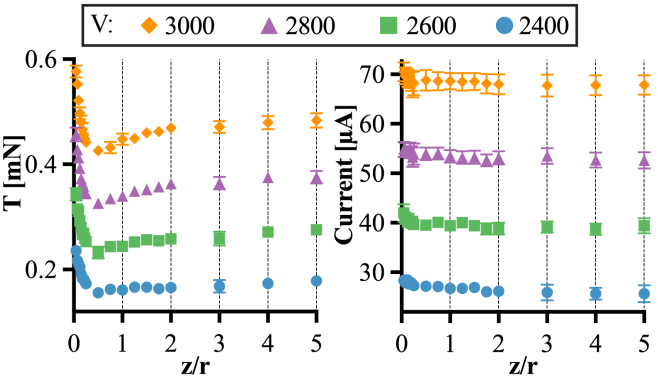

Fig. 5. Thrust versus z/r ratio (left) and current versus z/r ratio (right) at different applied voltages for a single thruster.

high voltage supply output monitor and from across a shunt resistor are recorded with a Rigol DS1054Z oscilloscope throughout each experimental trial (a voltage sweep up to ≈3kV) and used to calculate true applied voltage and output current.

IV. Results and Discussion

All experiments are performed with two devices per test condition and three trials per device. Plotted data is the overall mean (mean of each device's trial mean) with standard error of the mean (SEM) error bars.

A. Single thruster experiments

Experiments for the ground effect of a single thruster consider the dependent variables of thrust (T), ion current, ratio of thrust to out-of-ground-effect (OGE) thrust (T/T_0), and ratio of thrust efficiency (in N/W) to OGE efficiency (η/η_0), all with respect to z/r.

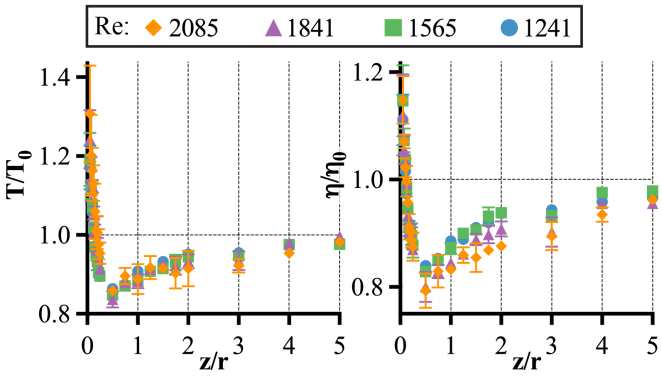

Fig. 6. Ratio of measured thrust to out-of-ground-effect thrust ($z/r >> 10$) versus z/r (left) and ratio of measured thrust efficiency to out-of-ground-effect thrust efficiency versus z/r (right) for a single thruster at different Reynolds numbers, calculated based on force data and simple momentum theory.

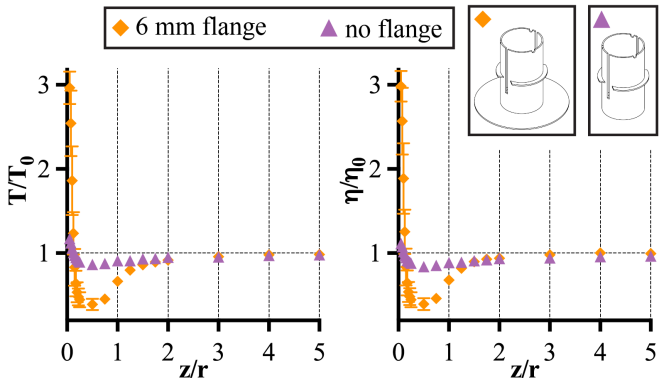

Fig. 7. Ratio of measured thrust to out-of-ground-effect thrust versus z/r (left) and ratio of measured thrust efficiency to out-of-ground-effect efficiency versus z/r (right) for a single thruster with and without inclusion of an exhaust flange. The approximately 2.5 mN/W out-of-ground-effect thrust efficiency rises to over 7 mN/W at low z/r ratios. All data collected at 3kV applied potential.

As expected, the measured thrust increases with applied voltage as the ion-accelerating drift field increases in magnitude (Fig. 5, left). Interestingly, the measured ion current at low z/r ratios also increases (Fig. 5, right) at the same applied voltage. We hypothesize that this is due to the increased magnitude of the convective term driving the ion current relative to the drift term; in ground effect, the increased velocity of the impinged wall jet should propagate through the device and increase inlet air velocity. For reference, the ion drift velocity (based on the formula $v_{drift} = \mu E$, where μ is the ion mobility and E is the field magnitude), is expected to be roughly 100 m/s at reasonable operating voltages.

Measured OGE thrust at different applied voltages can be used to calculate an approximate jet Reynolds number, where simple momentum theory is used to derive the average outlet air velocity via $T = 0.5\rho A v^2$. We show that, at least over the limited achievable range of these devices, ground proximity effects do not have a strong dependence on Reynolds number (Fig. 6). It is unlikely that any realistic centimeter-scale EAD thruster will be able to reach much higher outlet velocities and Reynolds numbers (i.e., $> 10^4$) past the

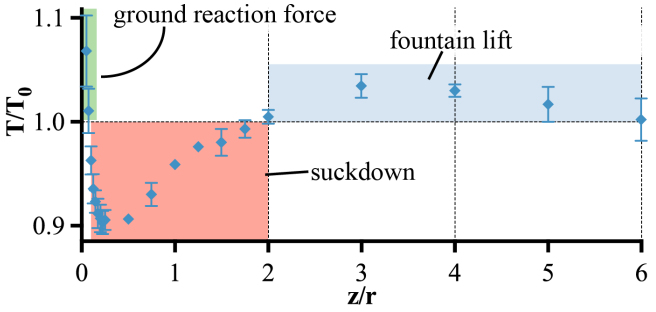

Fig. 8. Quadthruster data (s = 12 mm, h = 9 mm, 3kV applied potential) with hypothesized regions of dominant proximity effect shaded and labeled. The precise location and size of these regions is expected to shift depending on the specific thrusters and multi-thruster geometric configuration.

laminar-to-turbulent transition where we would definitely expect changes.

Proximity to the ground results in up to a 30% increase in thrust relative to OGE thrust (Fig. 6, left) at an applied voltage of 3 kV, in contrast to the $\approx 14\%$ found for small isolated rotors [21]. Additionally, whereas isolated rotors never drop below OGE thrust [21], [37], the thrust then falls and remains below OGE thrust from $z/r \approx 0.25$ until $z/r \approx 5$. This is similar to measurements made for (much larger) isolated jets from VTOL aircraft, which see an anomalous amount of suckdown under-predicted by existing analytical models [42], [43]. As a result of the increased ion current at low z/r ratios, the efficiency benefits are actually smaller than the thrust benefits (Fig. 6, right) by 10-20%. This effect disappears at higher z/r ratios, which supports the hypothesis that it is due to a proximity-induced increase in the convective current term (associated with v in Eq. 2).

Also considered is the effect of a circular flange extended 6 mm from the base of the thruster on the relative thrust and relative efficiency (Fig. 7). Our hypothesis, which is that the increased surface area of the flange will increase benefits at low z/r ratios due to an increased ground reaction force, but increase suckdown at higher z/r ratios due to increased fuselage area for suction pressure to act on, is supported by the data. In this case the relative importance of the hypothesized ion convection term is harder to see relative to the ground effect; the relative efficiency is identical to within measurement deviation.

B. Multi-thruster experiments

We also tested quadthruster configurations with varying inter-thruster spacing, s, thruster protrusion, h, and inclusion of aerodynamic strakes. For a visual reference of these parameters see Fig. 4, left. Now that multiple jets are present, fountain lift manifests as the dominant effect at high z/r ratios. All three (ground, suckdown, fountain) of the observed proximity effects are labeled with their dominant regions on top of a representative dataset in Fig. 8.

Figure 9 shows the measured thrust and current for a quadthruster at different applied voltages. Unlike the data for the single thruster, we do not see an increase in current at low z/r ratios, or if there is one it is within the measurement

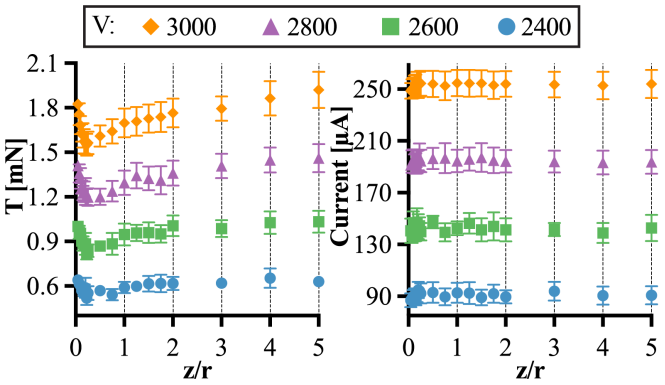

Fig. 9. Thrust versus z/r ratio (left) and current versus z/r ratio (right) at different applied voltages for a quadthruster with h = 9 mm and s = 20 mm.

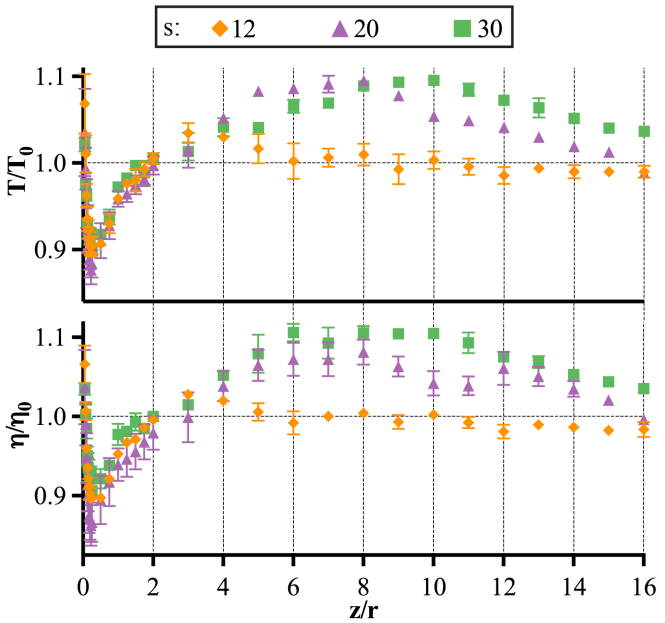

Fig. 10. Ratio of measured thrust to out-of-ground-effect thrust versus z/r for a quadthruster configuration with different inter-thruster spacing, s. All data collected at 3kV applied potential with h = 9 mm.

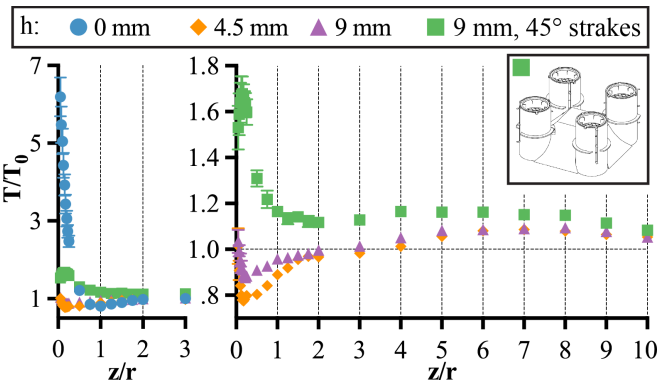

Fig. 11. Ratio of measured thrust to out-of-ground effect thrust versus z/r for a quadthruster configuration with different thruster protrusion heights, h, or inclusion of strakes (right). The same, but including h = 0 data, which significantly skews the range of the measured thrust enhancement (left). The approximately 2.5 mN/W out-of-ground-effect thrust efficiency rises to almost 4 mN/W for the straked design and over 10 mN/W for the flush fuselage h = 0 design at low z/r ratios. All data collected at 3kV applied potential with s = 20 mm.

error. One hypothesis is that the impinged wall jet velocity is decreased from a combination of mixing with the entrained fuselage airflow and mixing with neighboring jet exhausts, and as a result the convective ion flow term no longer becomes significant. This is a complicated effect requiring direct flow visualization to assess.

The inter-thruster spacing was shown to have a strong effect on the location and magnitude of the thrust enhancement attributable to fountain lift (Fig. 10). A possible explanation for why fountain lift is shown to continuing increasing until higher z/r ratios for increasing values of s is that those devices present a larger apparent surface area to the inner region where the exhaust streams intersect and are redirected upwards. The fountain jet is unlikely to be well collimated, as it has lost energy during redirection; much of the rising fountain lift airflow will just be pushed back to the ground plane by the jet exhausts at low spacing values. Importantly, the magnitude of the ground effect at very low z/r ratios is shown to never exceed 10% here, compared to about 30% for the single-thruster case (without flange). We hypothesize that this due to the increased magnitude of the suckdown effect due to the larger fuselage area of a quadthruster.

The magnitude of the suckdown effect relative to ground effect at low z/r ratios showed a strong dependence on thruster protrusion from the fuselage (Fig. 11). We hypothesize that suckdown is worse for the lower tested h value because the streamline around the fuselage is closer to the impinged wall jet, so it is entrained and accelerated more strongly. When h reaches 0 mm, however, there is no longer any space for the fuselage streamline to enter the underside of the device before being pushed out by wall jet, therefore there can be no force from a pressure differential across the fuselage (Fig. 11, left). The magnitude of the ground effect also rises dramatically when $h = 0$, although it is impossible to definitively say what percentage of that change is from removal of suckdown. This increase makes sense; the flat fuselage provides a larger surface area for the ground reaction pressure to act on, whereas at higher h values the fuselage is at effectively a higher z/r ratio than the thrusters.

Aerodynamic slats known as strakes are used on the underside of V/STOL aircraft to reduce the effect of suckdown (among other benefits) [28]. We show that surrounding the fuselage with 45° strakes which extend down to be flush with the thruster exhausts (Fig. 1) removes any suckdown effect, just like for the $h = 0$ case (Fig. 11, right); presumably, the streamlines follow the strakes and are unable to enter the underside of the device before being pushed out by the impinged wall jet. This data supports our hypothesis for the magnitude of the ground effect in the $h = 0$ case, because the rest of the fuselage is still elevated and a much more modest performance benefit is seen at low z/r ratios. This is the only configuration which never shows a performance decrease at any distance from the ground plane.

V. Limitations and Future Work

While this study shows how various geometric variables are useful for predicting and controlling ground proximity effects, this is a high-dimensional space and the physical phenomena are highly sensitive; a more rigorous experimental suite exploring the combinatorial geometric factors, for example using statistically-powered multi-factor analysis, is warranted in the future. As the fundamental physics governing performance are so different between EAD thrusters and motor-driven propellers, we have opted to compare findings qualitatively instead of try to adapt an existing model using unjustifiable fit parameters.

There are also several potentially interesting device parameters not explored here, including thruster radius, forward flight speed (or ambient flow velocity), and angle of attack. The maximum achievable and maximum change in Reynolds number were also limited by the operating range and number of stages in the devices. As related studies of rotorcraft and V/STOL aircraft note some dependence on all of these variables, we expect them to be important in future work.

Finally, our hypotheses about dominant proximity effect in each z/r region are supported by the data, but without direct flow measurement are impossible to fully confirm. Flow visualization using particle image velocimetry (PIV) or another similarly high-fidelity technique would be an interesting addition to future work, though it is unclear how adulteration of the ambient gas composition (e.g., with tracer particles or smoke) will affect EAD device performance.

VI. Conclusion

Understanding the influence of ground proximity effects on vehicle performance is critical for deploying them safely and efficiently in constrained environments. We show that there are significant effects to consider for small-scale electroaerodynamic propulsors depending on thruster geometry, multi-thruster arrangement, distance from the ground plane, and inclusion of exhaust flanges or fuselage strakes. These effects have the potential to either greatly improve efficiency in hover—for example, static thrust of a quadthruster was shown to increase by over 300% under certain conditions—or greatly reduce it—for example, static thrust was instead *reduced* by 20% in only a slightly different configuration, at the same distance from the ground plane. Compared to studies of small rotors, which follow similar trends but only see variations in static thrust on the order of 20%, this indicates proximity effects are critical to consider for operation of EAD-propelled vehicles [21]. The measured magnitude of efficiency enhancement from ground proximity effects helps close the gap between EAD actuators and flapping wings, bringing them within an order of magnitude ($\approx$ 10 mN/W). Our results point towards fruitful areas of future investigation for development of a model for these effects as they apply to EAD propulsion, and may open the door to power-autonomous ion-propelled vehicles designed to take advantage of proximity-based efficiency enhancement.

ACKNOWLEDGMENT

The authors would like to thank the staff and sponsors of the University of Utah Undergraduate Research Opportunity Program (UROP) for supporting author G.N..

REFERENCES

[1] F. Fraundorfer, L. Heng, D. Honegger, G. H. Lee, L. Meier, P. Tanskanen, and M. Pollefeys, "Vision-based autonomous mapping and exploration using a quadrotor MAV," in *2012 IEEE/RSJ International Conference on Intelligent Robots and Systems*, 2012, pp. 4557–4564, ISSN: 2153-0866.

[2] Q. Li, D.-C. Li, Q.-f. Wu, L.-w. Tang, Y. Huo, Y.-x. Zhang, and N. Cheng, "Autonomous navigation and environment modeling for MAVs in 3-d enclosed industrial environments," *Computers in Industry*, vol. 64, no. 9, pp. 1161–1177, 2013.

[3] S. Shen, N. Michael, and V. Kumar, "Autonomous multi-floor indoor navigation with a computationally constrained MAV," in *2011 IEEE International Conference on Robotics and Automation*, 2011, pp. 20–25, ISSN: 1050-4729.

[4] J. Quenzel, M. Nieuwenhuisen, D. Droeschel, M. Beul, S. Houben, and S. Behnke, "Autonomous MAV-based indoor chimney inspection with 3d laser localization and textured surface reconstruction," *Journal of Intelligent & Robotic Systems*, vol. 93, no. 1, pp. 317–335, 2019.

[5] T. Rouček, M. Pecka, P. Čížek, T. Petříček, J. Bayer, V. Šalanský, D. Heřt, M. Petrlík, T. Báča, V. Spurný, F. Pomerleau, V. Kubelka, J. Faigl, K. Zimmermann, M. Saska, T. Svoboda, and T. Krajník, "DARPA subterranean challenge: Multi-robotic exploration of underground environments," in *Modelling and Simulation for Autonomous Systems*, ser. Lecture Notes in Computer Science, J. Mazal, A. Fagiolini, and P. Vasik, Eds. Springer International Publishing, 2020, pp. 274–290.

[6] J. G. R. Iii, R. E. Sherrill, A. Schang, S. L. Meadows, E. P. Cox, B. Byrne, D. G. Baran, J. W. C. Iii, and K. M. Brink, "Distributed subterranean exploration and mapping with teams of UAVs," in *Ground/Air Multisensor Interoperability, Integration, and Networking for Persistent ISR VIII*, vol. 10190. SPIE, 2017, pp. 285–301.

[7] A. Eudes, J. Marzat, M. Sanfourche, J. Moras, and S. Bertrand, "Autonomous and safe inspection of an industrial warehouse by a multi-rotor MAV," in *Field and Service Robotics*, ser. Springer Proceedings in Advanced Robotics, M. Hutter and R. Siegwart, Eds. Springer International Publishing, 2018, pp. 221–235.

[8] M. Beul, N. Krombach, M. Nieuwenhuisen, D. Droeschel, and S. Behnke, "Autonomous navigation in a warehouse with a cognitive micro aerial vehicle," in *Robot Operating System (ROS): The Complete Reference (Volume 2)*, ser. Studies in Computational Intelligence, A. Koubaa, Ed. Springer International Publishing, 2017, pp. 487–524.

[9] W. Kwon, J. H. Park, M. Lee, J. Her, S.-H. Kim, and J.-W. Seo, "Robust autonomous navigation of unmanned aerial vehicles (UAVs) for warehouses' inventory application," *IEEE Robotics and Automation Letters*, vol. 5, no. 1, pp. 243–249, 2020.

[10] K. Karydis and V. Kumar, "Energetics in robotic flight at small scales," *Interface focus*, vol. 7, no. 1, p. 20160088, 2017.

[11] Y. Mulgaonkar, M. Whitzer, B. Morgan, C. M. Kroninger, A. M. Harrington, and V. Kumar, "Power and weight considerations in small, agile quadrotors," in *Micro- and Nanotechnology Sensors, Systems, and Applications VI*, vol. 9083. International Society for Optics and Photonics, 2014, p. 90831Q.

[12] D. S. Drew, N. O. Lambert, C. B. Schindler, and K. S. J. Pister, "Toward controlled flight of the ionocraft: A flying microrobot using electrohydrodynamic thrust with onboard sensing and no moving parts," *IEEE Robotics and Automation Letters*, vol. 3, no. 4, pp. 2807–2813, 2018.

[13] H. Zhang, J. Leng, D. Liu, Z. Liu, D. Huang, M. Qi, and X. Yan, "Low voltage control of micro-ionic thrusters using the electrostatic induced potential of the collector," *IEEE Robotics and Automation Letters*, vol. 6, no. 4, pp. 6884–6890, 2021.

[14] H. K. H. Prasad, R. S. Vaddi, Y. M. Chukewad, E. Dedic, I. Novosselov, and S. B. Fuller, "A laser-microfabricated electrohydrodynamic thruster for centimeter-scale aerial robots," *PLOS ONE*, vol. 15, no. 4, p. e0231362, 2020.

[15] H. Zhang, J. Leng, D. Liu, W. Zhan, R. Yun, Z. Liu, M. Qi, and X. Yan, "A centimeter-scale electrohydrodynamic multi-modal robot capable of rolling, hopping, and taking off," *IEEE Robotics and Automation Letters*, vol. 7, no. 4, pp. 11 791–11 798, 2022.

[16] A. Wojciechowska, J. Frey, E. Mandelblum, Y. Amichai-Hamburger, and J. R. Cauchard, "Designing drones: Factors and characteristics influencing the perception of flying robots," *Proceedings of the ACM on Interactive, Mobile, Wearable and Ubiquitous Technologies*, vol. 3, no. 3, pp. 1–19, 2019.

[17] J. Goh, J. Pfeffer, S. A. Zenios, and S. Rajpal, "Workplace stressors & health outcomes: Health policy for the workplace," *Behavioral Science & Policy*, vol. 1, no. 1, pp. 43–52, 2015.

[18] A. C. Costa, "Work team trust and effectiveness," *Personnel Review*, vol. 32, no. 5, pp. 605–622, 2003.

[19] B. Schäffer, R. Pieren, K. Heutschi, J. M. Wunderli, and S. Becker, "Drone noise emission characteristics and noise effects on humans—a systematic review," *International Journal of Environmental Research and Public Health*, vol. 18, no. 11, p. 5940, 2021.

[20] A. W. Christian and R. Cabell, "Initial investigation into the psychoacoustic properties of small unmanned aerial system noise," in *23rd AIAA/CEAS Aeroacoustics Conference*. American Institute of Aeronautics and Astronautics, 2021, _eprint: https://arc.aiaa.org/doi/pdf/10.2514/6.2017-4051.

[21] S. A. Conyers, M. J. Rutherford, and K. P. Valavanis, "An Empirical Evaluation of Ground Effect for Small-Scale Rotorcraft," in *2018 IEEE International Conference on Robotics and Automation (ICRA)*, May 2018, pp. 1244–1250, iSSN: 2577-087X.

[22] K. D. von Ellenrieder, K. Parker, and J. Soria, "Fluid mechanics of flapping wings," *Experimental Thermal and Fluid Science*, vol. 32, no. 8, pp. 1578–1589, 2008.

[23] D. S. Drew and S. Follmer, "High force density multi-stage electrohydrodynamic jets using folded laser microfabricated electrodes," in *2021 21st International Conference on Solid-State Sensors, Actuators and Microsystems (Transducers)*, 2021, pp. 54–57, ISSN: 2167-0021.

[24] C. L. Nelson and D. S. Drew, "High aspect ratio multi-stage ducted electroaerodynamic thrusters for micro air vehicle propulsion," 2023.

[25] L. Pekker and M. Young, "Model of ideal electrohydrodynamic thruster," *journal of propulsion and power*, vol. 27, no. 4, pp. 786–792, 2011.

[26] K. Masuyama and S. R. Barrett, "On the performance of electrohydrodynamic propulsion," *Proceedings of the Royal Society A: Mathematical, Physical and Engineering Sciences*, vol. 469, no. 2154, p. 20120623, 2013.

[27] P. Sanchez-Cuevas, G. Heredia, and A. Ollero, "Characterization of the aerodynamic ground effect and its influence in multirotor control," *International Journal of Aerospace Engineering*, vol. 2017, p. e1823056, 2017.

[28] B. W. McCormick, *Aerodynamics of V/STOL Flight*. Courier Corporation, Jan. 1999.

[29] K. V. Rozhdestvensky, "Wing-in-ground effect vehicles," *Progress in Aerospace Sciences*, vol. 42, no. 3, pp. 211–283, 2006.

[30] T. V. Truong, D. Byun, M. J. Kim, K. J. Yoon, and H. C. Park, "Aerodynamic forces and flow structures of the leading edge vortex on a flapping wing considering ground effect," *Bioinspiration & Biomimetics*, vol. 8, no. 3, p. 036007, 2013.

[31] L. Long and J. G. Wong, "On the origin of the ground effect," *International Journal of Mechanical Engineering Education*, p. 03064190231174438, May 2023.

[32] P. Bevilaqua, R. Margason, and C. Gaharan, "A Jet Entrainment Theory for VTOL Aircraft Suckdown," in *45th AIAA Aerospace Sciences Meeting and Exhibit*. Reno, Nevada: American Institute of Aeronautics and Astronautics, Jan. 2007.

[33] R. E. Kuhn, "Hover Suckdown and Fountain Effects," Dec. 1987, p. 872305.

[34] K. Yen, "Vertical momentum of the fountain produced by multijet vertical impingement on a flat ground plane," *Journal of Aircraft*, vol. 18, no. 8, pp. 650–654, Aug. 1981.

[35] I. C. Cheeseman and W. E. Bennet, "The effect of the ground on a helicopter rotor in forward flight," 1955.

[36] H. N. J. Dekker, D. Ragni, W. J. Baars, F. Scarano, and M. Tuinstra, "Aerodynamic Interactions of Side-by-Side Rotors in Ground Proximity," *AIAA Journal*, vol. 60, no. 7, pp. 4267–4277, July 2022.

[37] T. Jardin, S. Prothin, and C. G. Magaña, "Aerodynamic Performance of a Hovering Microrotor in Confined Environment," *Journal of the American Helicopter Society*, vol. 62, no. 2, pp. 1–7, Apr. 2017.

[38] A. Matus-Vargas, G. Rodriguez-Gomez, and J. Martinez-Carranza, "Ground effect on rotorcraft unmanned aerial vehicles: a review," *Intelligent Service Robotics*, vol. 14, no. 1, pp. 99–118, Mar. 2021.

[39] Y. H. Hsiao and P. Chirarattananon, "Ceiling effects for hybrid aerial–surface locomotion of small rotorcraft," *IEEE/ASME Transactions on Mechatronics*, vol. 24, no. 5, pp. 2316–2327, 2019.

[40] R. Ding, Y.-H. Hsiao, H. Jia, S. Bai, and P. Chirarattananon, "Passive wall tracking for a rotorcraft with tilted and ducted propellers using

proximity effects," *IEEE Robotics and Automation Letters*, vol. 7, no. 2, pp. 1581–1588, 2022.

[41] Y.-H. Hsiao, S. Bai, Y. Zhou, H. Jia, R. Ding, Y. Chen, Z. Wang, and P. Chirarattananon, "Energy efficient perching and takeoff of a miniature rotorcraft," *Communications Engineering*, vol. 2, no. 1, pp. 1–14, 2023.

[42] R. E. Kuhn, D. C. Bellavia, V. R. Corsiglia, and D. A. Wardwell, "On the estimation of jet-induced fountain lift and additional suckdown in hover for two-jet configurations, Tech. Rep. NAS 1.15:102268, Aug. 1991, nTRS Author Affiliations: STO-VL Technology, NASA Ames Research Center NTRS Document ID: 19920024374 NTRS Research Center: Legacy CDMS (CDMS).

[43] D. C. Bellavia, D. A. Wardwell, V. R. Corsiglia, and R. E. Kuhn, "Suckdown, fountain lift, and pressures induced on several tandem jet V/STOL configurations, Tech. Rep. NASA-TM-102817, Mar. 1991, nTRS Author Affiliations: NASA Ames Research Center, STO-VL Technology NTRS Document ID: 19910014795 NTRS Research Center: Legacy CDMS (CDMS).